Design and characterization of small thermoelectric generators for environmental monitoring devices

# Design and characterization of small thermoelectric generators for environmental monitoring devices

R. Bonin [a,c,*], D. Boero [a,c], M. Chiaberge [b,c], A. Tonoli [a,c]

[a] DIMEAS, Politecnico di Torino, 10129 Torino, Italy
[b] DET, Politecnico di Torino, 10129 Torino, Italy
[c] Laboratorio di Meccatronica, Politecnico di Torino, 11029 Verrès (AO), Italy

A B S T R A C T

A small thermoelectric generator to power autonomous sensors in remote environmental sites is studied, designed, realized, characterized, and tested. The thermoelectric phenomena, applied to our device, are theoretically introduced and experimentally verified by directly measuring the physical quantities when the thermoelectric generator operates in working conditions. The device is then tested under different external conditions, showing that it is able to supply, for sufficient long time, an output voltage higher than 200 mV and an output power on the order of 10 mW when a temperature difference higher than 10 K and a load resistance close to the internal resistance are considered. Furthermore we developed a devoted power conditioning circuit in order to usefully manage the output voltage. Finally, we tested the device in real operative conditions.

## 1. Introduction

During the last 20 years the request of renewable and environmentally ''green'' sources of energy in order to deal with the problem of pollution and global warming has been noticeably increased. In particular, parts of these studies are focused on the pursuit of energy harvesting from unused sources like mechanical vibrations and wasted heat. Within these researches, the applica-tions which involve the thermoelectric phenomena have been intensively developed [1–5]. In more details, the thermoelectric modules are solid-state devices commonly used in cooling/heating applications, but in the last years they have been largely studied and utilized as energy converters since they are able to produce electricity from heat absorption. In particular, small thermoelectric generator devices are principally used to power localized autono-mous sensors, but their fields of application are at this time re-stricted to aero-spatial and automotive industries.

Within this framework, in this paper we extend the area of interest for the employment of thermoelectric generators to the environmental monitoring. The use of large thermoelectric generators in remote sites started since the sixties of the previous century in order to power data acquisition equipments and communication devices, such as weather stations, navigation aids, and subsea operations [6]; in all these cases the heat source was powered by either radioisotopes or fossil fuels. In our work we studied, designed, realized, and characterized a small thermoelectric generator in order to supply energy to autonomous sensors, placed in remote locations with hard environmental conditions (very low temperature, difficult access, etc.), where the usual renewable energy sources, like solar and wind energy, are not regularly available.

The novelty of our work, with respect to the previously mentioned devices and the known applications discussed in literature, has to be found both in the originality of the proposed device, by considering in particular its whole structure, and the field of application. Furthermore, this thermoelectric generator has been completely realized, optimized, and characterized after having considered both the physical models for thermoelectric phenomena and its specific practical applications. As first consideration, we highlight the peculiarity of the heat source employed since in our case the heat is supplied by a flameless catalytic burner. Such type of heat source has been already studied [7,10], but only in laboratory tests, without any sort of applications in real operative conditions. This kind of heat source is more competitive and reliable with respect to flame burner when it is used for applications where low power and small dimensions are required. In addition, our study permits to model our thermoelectric generator when different natural heat sources are considered since the employed catalytic burner basically provides a low-temperature heat source, exactly what we expect from renewable heat sources as geothermal, ocean thermal energy, and waste heat to mention few ones [6]. Secondly, the comparison between the physical model and

* Corresponding author at: DIMEAS, Politecnico di Torino, 10129 Torino, Italy. Tel.: +39 0125922538; fax: +39 0125922539.
*E-mail address:* roberto.bonin@polito.it (R. Bonin).

the experimental studies [15,14,11,9] of thermoelectric generators as well as their performances [8] under different operative conditions have been extensively developed but only in the ideal laboratory conditions. In our work, all the experimental tests have been worked out by using the device in its real operative layout. Moreover, the situations actually found in realistic operative conditions are mainly studied theoretically [12], whereas the realistic experimental tests are principally developed by considering residential applications [13] or devices assembled with large parts [6]. Here, we have extensively tested our small prototype under realistic environmental conditions, the same ones which it can find when it effectively operates in the required applications. Finally, we remark that the power conditioning electric module is generally neglected in thermoelectric generator demonstrations, whereas in this work it plays a fundamental role.

This paper is organized as it follows. After having introduced the thermoelectric phenomena we recall their basic physical mod-el. Subsequently, we describe the design of the whole thermoelec-tric generator. In particular, we discuss in details the power conditioning external circuit, developed in order to correctly use the output voltage as energy supply for autonomous sensors. Then, we illustrate the experimental measurements carried out both to test the validity of the physical model previously discussed and to check the capability of our device to be reasonably used in the expected environment. Finally, we show the results obtained during the tests carried out in real operative conditions. By summarizing, we have designed and realized a complete thermoelectric generator powered by a flameless catalytic burner; the device has been tested both in laboratory, by comparing the experimental results with the theoretical predictions, and in real environmental situations, by proving its capability to be used as power generator for environmental monitoring sensors.

## 2. Physical models

Thermoelectric (TE) phenomena are basically observed when two different materials are joined together and they are either subjected to a temperature gradient or crossed by an electrical current [6]. In particular, the Seebeck effect describes the generation of a voltage difference $\Delta V$ when the two sides of the junction are held at different temperature $\Delta T$, showing a proportional dependence given by $\Delta V = \alpha \Delta T$, where $\alpha$ is the Seebeck coefficient or thermopower. The inverse effect, the Peltier effect, arises when an electrical current passes through the junction of two different materials, with the consequent heat absorption or rejection, depending on the current direction. The heat flow is proportional to the current $I$ as $dQ/dt = \Pi I$, being $\Pi$ the Peltier coefficient which Thomson (Lord Kelvin) proved to be proportional to the absolute temperature $\Pi = \alpha T$. A further TE effect, the Thomson effect, describes the heat production (absorption or emission) of an electrical current in a single material under the presence of a temperature gradient. By the way, the Seebeck, Peltier, and Thomson effects are reversible, whereas the Joule effect is obviously not.

Modern TE refrigeration devices and TE power generation devices are based on Peltier and Seebeck effects, respectively; their core is made by thermoelectric couples composed of n-type and p-type semiconductors (basically, $Bi_2Te_3$ and $Si_{1-x}Ge_x$) pellets connected by metallic electrical contact pads. In such devices, a large number of these thermoelectric couples are connected electrically in series and thermally in parallel. Thermocouples are then placed between two ceramic plates which are electrically insulating and thermally conducting. An example of TE module (TEM) is shown in Fig. 1. Thermal energy is supplied by the heat source at temperature $T_H$ which drops at temperature $T_{HJ}$ at the hot thermocouples junctions due to the finite thermal conductance $K$ of the ceramic

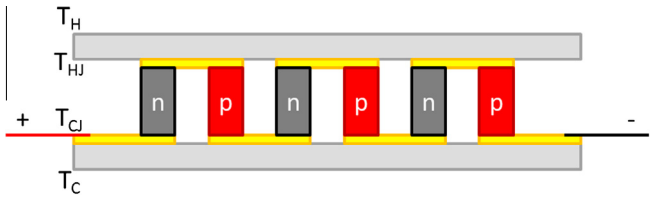


**Fig. 1.** Sketch of TEM. Grey surfaces: ceramic plates; +/−: electrode terminals; yellow lines: electrical connections; black and red bars: n- and p-type semiconductors; $T_H$: temperature of heat source; $T_C$: temperature of heat sink; $T_{HJ}$: temperature of hot junction; $T_{CJ}$: temperature of cold junction. (For interpretation of the references to color in this figure legend, the reader is referred to the web version of this article.)

plates. For the same reason, the cold junction remains at the temperature $T_{CJ}$, whereas at the heat sink we recover the lower temperature $T_C$. We therefore define the two temperature differences [14] as $\Delta T = T_H - T_C$ and $\Delta T_{\text{eff}} = T_{HJ} - T_{CJ}$.

Geometrically, TEMs are characterized by the cross sectional area $A$ of ceramic plates, the thickness $H$ of the whole TEM, the cross sectional area $A_s$ and the height $h$ of each pellet, the height $h' = (H - h)/2$ of each ceramic plate, and the number $N$ of thermocouples. The thermal conductance $K$ of ceramic plates is given by $K = k_c A/h'$, where $k_c$ is the thermal conductivity of the ceramic whose value is in the range (18–36) W/Km for $Al_2O_3$, typically used in TEMs applications. Besides, the other properties of the TEM are the internal thermal conductance $K_{in} = 2Nk_sA_s/h$ and the internal electrical resistance $R_{in} = 2N\rho_s h/A_s$, where $k_s$ (typically 1.5–2.0 W/Km) and $\rho_s$ are the thermal conductivity and the electrical resistivity of a single pellet, respectively (for the corresponding values in literature see, e.g., [6,16,15]). Without loss of generality, we have considered the same thermal and electrical properties for both n- and p-type semiconductors; different properties can be eventually taken into account.

In the sequel, we will consider the simplest and most commonly used model to test an ideal TEG (see Ref. [6] for a detailed discussion). This classical method is based on the assumption that all the physical coefficients are constant and temperature independent, consequently the Thomson effect is neglected. Although its simplicity, this method has been successfully used to model a large variety of applications (e.g., see Refs. [15,14]). Nevertheless, we notice that more complete and detailed models have been extensively studied and experimentally verified [16,17]. On the other hand, this analysis is beyond the aim of our work and therefore it will not be considered.

The heat flow provided by the thermal source and flowing through the ceramic plate is [14]:

$$\dot{Q}_H = K(T_H - T_{HJ}), \quad (1)$$

whereas the heat flowing from the thermocouples to the external heat sink is:

$$\dot{Q}_C = K(T_{CJ} - T_C). \quad (2)$$

The voltage generated by the TEG is:

$$V_T = N(\alpha_p - \alpha_n)(T_{HJ} - T_{CJ}) = \alpha \Delta T_{\text{eff}}, \quad (3)$$

being $\alpha_p$, $\alpha_n$, and $\alpha = N(\alpha_p - \alpha_n)$ the Seebeck coefficients of p- and n-type semiconductors and of the whole TEG, respectively, and $\alpha_{pn} = (\alpha_p - \alpha_n)$ is the Seebeck coefficient of the single thermocouple. In case of open electrical circuit, the rate of the heat flowing through the thermocouples is simply $\dot{Q}_{in} = K_{in}(T_{HJ} - T_{CJ})$. Let us consider now a closed circuit where the variable load resistance $R_L$ is con-nected to the TEG electrodes (see Fig. 2) and consequently an electrical current $I$ flows in the circuit. In this case, it can be shown [6]

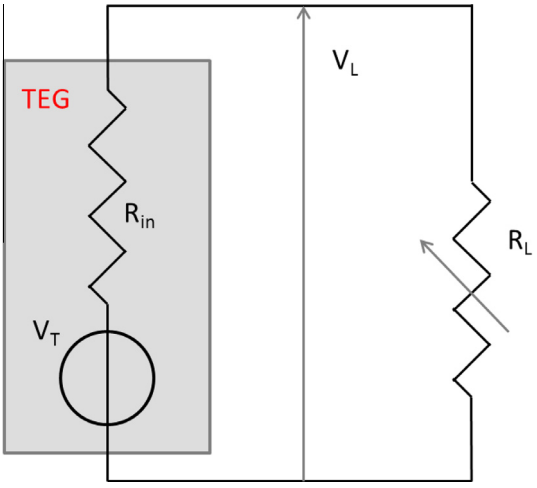


**Fig. 2.** Scheme of the circuit considered in the physical model. $V_T = \alpha\Delta T_{\text{eff}}$, $R_{in}$: internal resistance, $R_L$: variable load resistance.

that the rate of heat absorbed and the rate of heat dissipated are respectively:

$$\dot{Q}_H = \alpha T_{HJ} I + K_{in}\Delta T_{\text{eff}} - \frac{1}{2}R_{in}I^2, \tag{4}$$

$$\dot{Q}_C = \alpha T_{CJ} I + K_{in}\Delta T_{\text{eff}} + \frac{1}{2}R_{in}I^2, \tag{5}$$

where:

$$I = \frac{V_T}{R_{in} + R_L}. \tag{6}$$

The term proportional to $I$ is due to the Peltier effect, whereas the term proportional to $I^2$ takes into account the Joule effect (the factor 1/2 arises from the boundary conditions of the heat

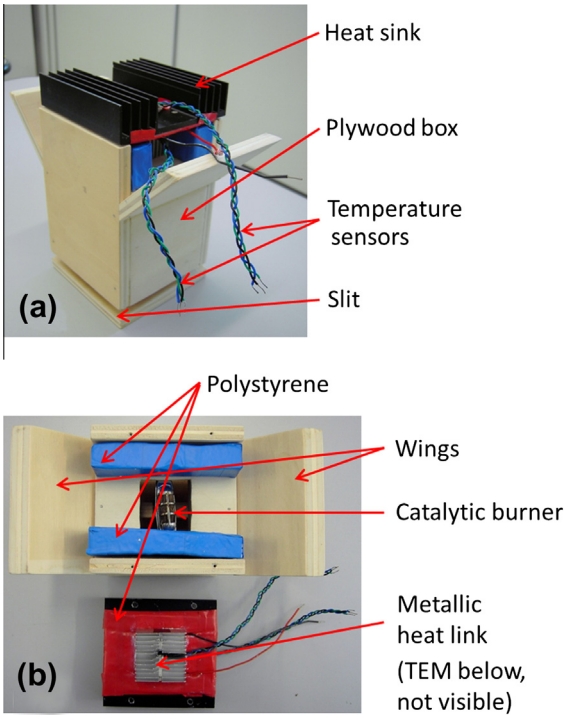


**Fig. 3.** Picture of the device (box + heat source + TEM). (a) Operative shape. (b) Open view.

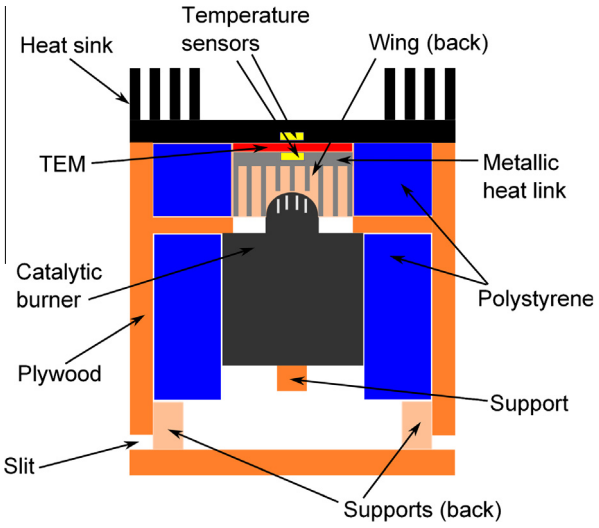


**Fig. 4.** Schematic section of the device (box + heat source + TEM).

transport equation [6]). According to this circuit and by writing the load resistance in term of internal resistance as $R_L = mR_{in}$ ($m$ is the proportional coefficient [15]) the output power $P_L$ supplied by the TEG is:

$$P_L = V_L I = N^2\alpha_{pn}^2\Delta T_{\text{eff}}^2 \frac{m}{R_{in}(1+m)^2}, \tag{7}$$

where $V_L$ is the voltage across $R_L$ and Eq. (6) has been considered. Eq. (7) clearly shows that the maximum power is obtained when the load resistance matches the internal resistance, that is, $m = 1$, $R_L = R_{in}$.

The relationship between $\Delta T$ and $\Delta T_{\text{eff}}$ is determined by considering that, at the equilibrium, the heat rates flowing through the ceramic plates are coincident with the heat rates absorbed and dissipated by the thermocouples, giving [14]:

$$\Delta T_{\text{eff}} = \frac{K}{K + 2K_{in} + \frac{2N^2\alpha_{pn}^2 T_M}{R_{in}+R_L}}\Delta T = \beta\Delta T, \tag{8}$$

where $T_M = (T_H + T_C)/2$ is the mean temperature. The term in the denominator containing the Seebeck coefficient describes the temperature change due to the Peltier effect, which depends on the current and consequently on the load resistance. However, as we are showing in the sequel, this term is small and can be reasonably neglected.

The TEG efficiency $\eta$ is defined as the ratio between the output power $P_L$ and the absorbed heat rate $\dot{Q}_H$ (see Eqs. (7) and (4)). Therefore we obtain:

$$\eta(m) = \frac{P_L}{\dot{Q}_H} = \frac{2mZ(T_{HJ} - T_{CJ})}{2(1+m)^2 + Z(T_{HJ} + 2mT_{HJ} + T_{CJ})}, \tag{9}$$

where the figure-of-merit $Z$ is defined by:

$$Z = \frac{N^2\alpha_{pn}^2}{K_{in}R_{in}}. \tag{10}$$

The efficiency at the matched load ($m = 1$) is equal to:

**Table 1**
Parameters of the thermoelectric module obtained from its data sheet.

| $N$ | $V_{DC}$ (V) | $R_{in}$ (Ω) | $I_{MAX}$ (A) | $P_{MAX}$ (W) | $T_{MAX}$ (C) | $W$ (mm) | $L$ (mm) | $H$ (mm) |
|---|---|---|---|---|---|---|---|---|
| 127 | 9.40 | 4.30 | 1.09 | 5.10 | 250 | 40 | 40 | 3.8 |

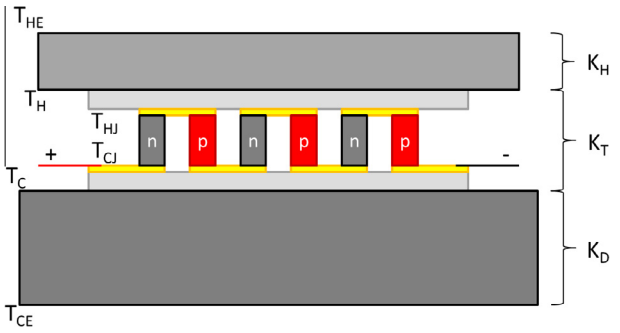


**Fig. 5.** Scheme of heat source (top), TEM (middle), and heat sink (bottom). $T_{HE}$: temperature of heat source at the catalytic burner side; $T_H$: temperature of heat source at the TEM side; $T_{CE}$: temperature of heat sink at the open side; $T_C$: temperature of heat sink at the TEM side; $T_{HJ}$: temperature of hot junction; $T_{CJ}$: temperature of cold junction. $K_H$, $K_T$, and $K_D$ represent the thermal conductances of metallic link, whole TEM, and heat sink, respectively.

$$\eta_{\text{match}} = \frac{1}{2}\frac{T_{HJ}-T_{CJ}}{T_{HJ}-\frac{1}{4}(T_{HJ}-T_{CJ})+\frac{2}{Z}}, \tag{11}$$

whereas the maximum efficiency, obtained when $m = m_{MAX} = \sqrt{1+ZT_M}$, is given by:

$$\eta_{\text{MAX}} = \frac{T_{HJ}-T_{CJ}}{T_{HJ}}\frac{\sqrt{1+ZT_M}-1}{\sqrt{1+ZT_M}+\frac{T_{CJ}}{T_{HJ}}}, \tag{12}$$

showing that the Carnot efficiency $\eta_C = (T_{HJ}-T_{CJ})/T_{HJ}$ is dropped by a term which depends on the figure-of-merit.

## 3. Design and realization of TEG device

The realized device is characterized by the following parts: (i) box; (ii) heat source; (iii) TEM; and (iv) external energy conversion circuit. A picture of the whole device (without external circuit) is shown in Fig. 3, whereas a schematic section is shown in Fig. 4.

### 3.1. Box

The aim of the box is to support all the parts of the device and to maximize the heat transport from the heat source to the TEM. In particular, it is a handmade rectangular box made with plywood sheets 1 cm thick. The cross section is rectangular (100 mm × 98 mm), coincident with the cross section of the heat sink, whereas two opposite sides are longer than the other ones (100 mm × 133 mm and 98 mm × 99 mm) to support the heat sink. The upper cap is fixed on the top of shorter faces and it has a square hole in the middle with the same lateral dimensions of the TEM. The lower cap is fixed to the box body in order to leave a slit along the whole basis perimeter; such opening ensures the necessary air flow required by the heat source, without loss of functional heat. Two additional "wings" have been fixed on the surfaces of short faces in order to protect the TEM and the heat source from external unrequired air flow. Inside the box we added polystyrene to stress the adiabatic properties.

### 3.2. Heat source

As heat source we have considered a flameless catalytic burner, which in our prototype is a simple commercial Zippo™ hand warmer [18]. Such burner uses fuel for lighters which releases heat through a reaction with a platinum catalyst. At room temperature and in an open space, the hand warmer cap surface reaches the maximum temperature of 75 °C ca. The hand warmer is placed inside the box with the burner exiting from the hole of the upper cap. In the box, the bottom slit and the upper hole guarantee the correct oxygen supply to the catalytic burner.

### 3.3. Thermoelectric module

The TEM used in our device is the commercial GM250-127-14-16 of European Thermodynamics [19]. Data sheet gives the parameters shown in Table 1. TEM is tested at the hot side temperature of 250 °C and at the cold side temperature of 50 °C. $N$ is the number of thermocouples, $V_{DC}$ the maximum voltage at open circuit, $R_{in}$ the internal resistance, $I_{MAX}$ the maximum current, $P_{MAX}$ the maximum power, and $T_{MAX}$ the maximum temperature of the hot surface. $W$ and $L$ are the width and the length of the ceramic plates, respectively. Direct measurements give $h$ = 2.2 mm, $h'$ = 0.8 mm, and $l$ = 1.5 mm.

To transfer the heat from the catalytic burner to the hot side of the TEM we used an aluminum heat sink between the heat source and the TEM. The heat sink is fin type with the same cross section of the TEM's one. The fins were cut with an appropriate shape to place the burner close to the TEM. The heat rejected by the TEM flows through a heat sink placed on the top of the box, fixed to the higher box's faces. This heat sink constitutes the cold side of the TEM. Polystyrene has been placed around the TEM to thermally insulate it.

Let us discuss how to optimize the relative dimensions of hot side heat sink, TEM, and cold side heat sink. By considering Fig. 5, we introduce the temperatures $T_{HE}$ (temperature of heat source at the catalytic burner side) and $T_{CE}$ (temperature of heat sink at the open side) and the thermal conductivities $K_H$, $K_T$, and $K_D$ of metallic link, whole TEM, and heat sink, respectively. In particular, $1/K_T = 1/K + 1/K_{in} + 1/K$ and consequently $K_T = K_{in}K/(K + 2K_{in})$. By assuming a perfect thermal insulation along the lateral faces and by neglecting thermal convection and irradiation,

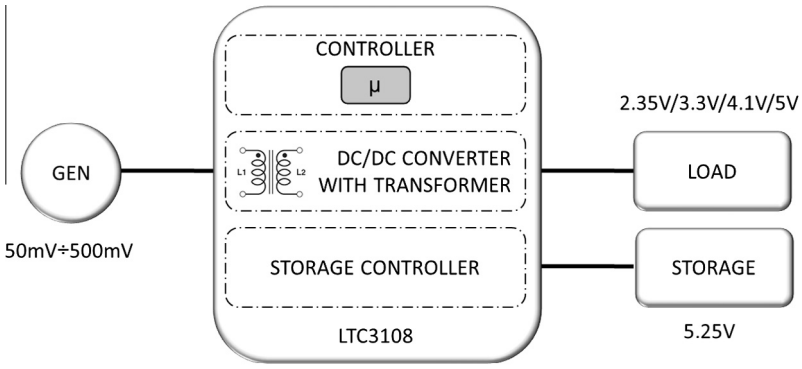


**Fig. 6.** Block diagram of the integrated solution with LT components.

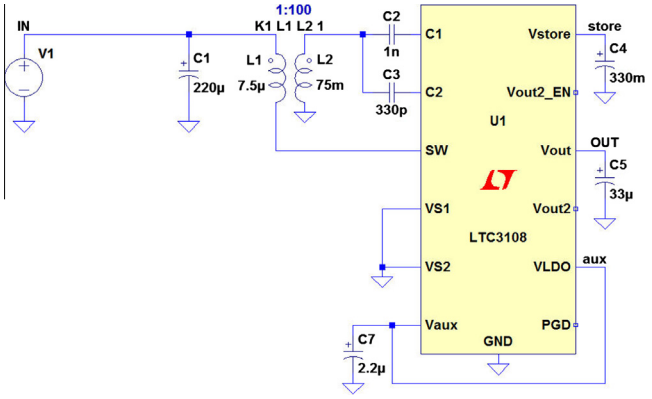


**Fig. 7.** Equivalent electronic circuits.

in open-circuit condition the heat conduction along the TEG is governed by the following equations:

$$K_H(T_{HE} - T_H) = K_T(T_H - T_C), \tag{13}$$

$$K_T(T_H - T_C) = K_D(T_C - T_{CE}). \tag{14}$$

By combining the two equations and by rearranging the terms, after having introduced the notations $\Delta T_E = T_{HE} - T_{CE}$ and $1/K_{\text{eff}} = 1/K_H + 1/K_T + 1/K_D$ and the additional equation $K_D(T_C - T_{CE}) = K_{\text{eff}}(T_{HE} - T_{CE})$, we obtain the following relationship:

$$\Delta T = \frac{1}{1 + \frac{K_T}{K_H} + \frac{K_T}{K_D}} \Delta T_E. \tag{15}$$

The TEG's design is optimized when the difference between $\Delta T$ and $\Delta T_E$ is as small as possible. Let us write the thermal conductance as $K_i = k_i A_i / h_i$, $i = H, T, D$, where $k_i$, $A_i$, and $h_i$ are the thermal conductivity, the cross sectional area, and the height of the corresponding element in the TEG, where the shape of a simple rectangular parallelepiped is considered (for sake of simplicity in the notation, we have temporarily introduced a subscript for the geometrical parameters concerning to the TEM). Besides, we reasonably assume that $k_H \simeq k_D$. Through these considerations we write:

$$\Delta T = T_H - T_C = \frac{1}{1 + \frac{k_T}{k_H}\left(\frac{A_T}{A_D}\frac{h_D}{h_T} + \frac{A_T}{A_H}\frac{h_H}{h_T}\right)} \Delta T_E. \tag{16}$$

A further consideration should be done: since all the thermocouples have to receive the maximum available amount of heat without any dispersion in the environment, we must have $A_T \simeq A_H$. Therefore, for given $k_T$ and $k_H$ we have to fulfill the conditions $A_T/A_D \ll 1$ and $h_D/h_T \ll 1$ in order to minimize the difference between $\Delta T$ and $\Delta T_E$.

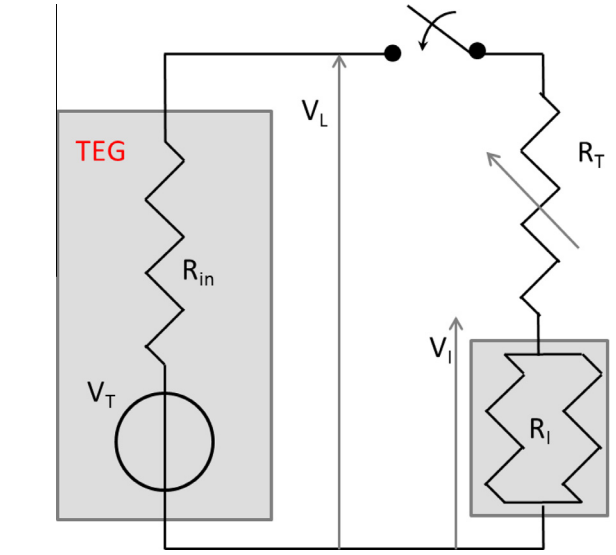


**Fig. 9.** Scheme of the circuit used to characterize the TEM. $V_T = \alpha\Delta T_{\text{eff}}$, $R_{in}$: internal resistance, $R_L = R_T + R_I$: variable load resistance. $R_I$ is made by two resistances in parallel.

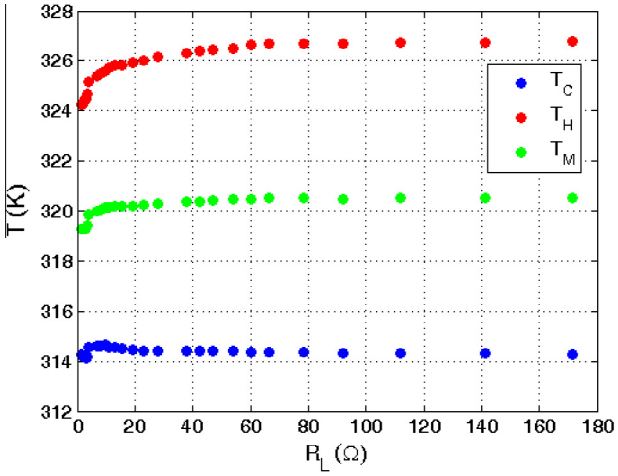


**Fig. 10.** Dependence of $T_C$, $T_H$, and $T_M$ on the load resistance.

### 3.4. External energy conversion circuit

In order to properly manage the energy produced by the generator, it is necessary to consider that our system, when switched on, starts to produce energy till the end of the fuel also if no load uses

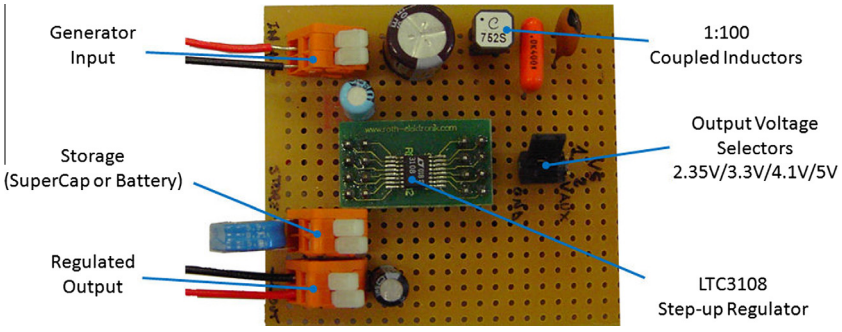


**Fig. 8.** Prototype of the energy conversion circuit.

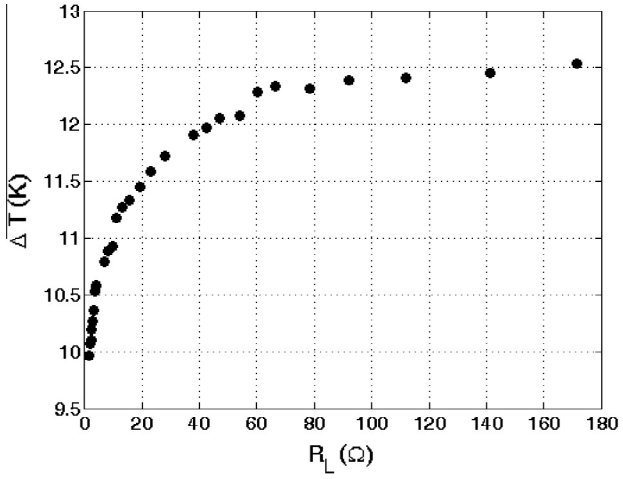


**Fig. 11.** Dependence of $\Delta T$ on the load resistance.

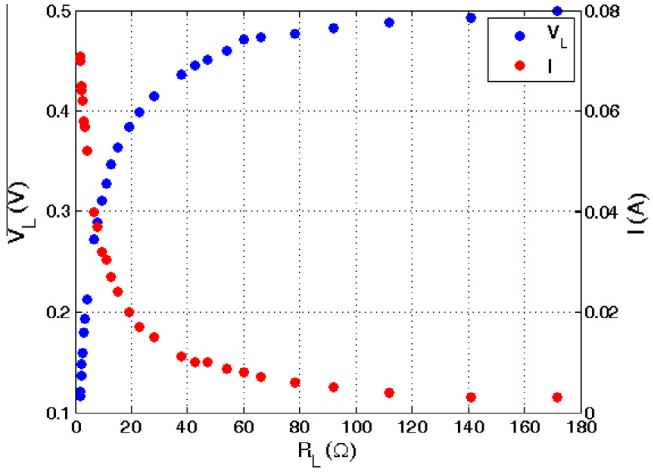


**Fig. 12.** Dependence of $V_L$ (blue dots, left axis) and $I$ (red dots, right axis) on the load resistance. (For interpretation of the references to color in this figure legend, the reader is referred to the web version of this article.)

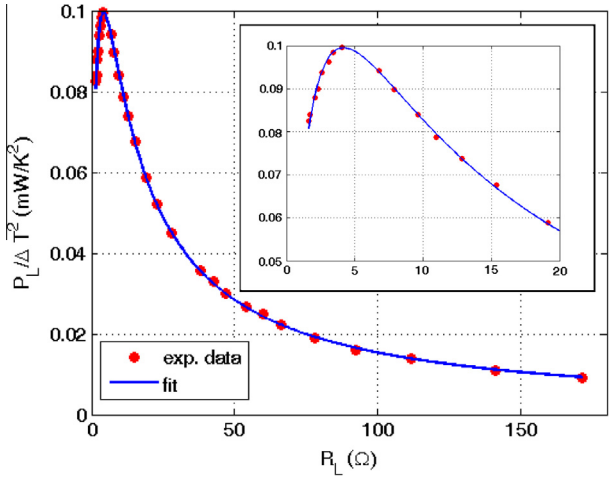


**Fig. 13.** Output power $P_L$ normalized by $\Delta T^2$ as a function of load resistance $R_L$. Red points: experimental data; blue line: data fit. Inset: magnified view around maximum. (For interpretation of the references to color in this figure legend, the reader is referred to the web version of this article.)

that energy. The best solution is not only to convert this energy to be used with the most part of microprocessors or sensors available on the market, but also to store that part of the energy that is not instantly used. Due to this limitation it is important to design a control system that can monitor, manage, and store the energy in order to increase the efficiency of the whole system. For this reason the energy converter can be divided into three different subsystems: (i) DC/DC regulator; (ii) control system; and (iii) storage system. By using thermoelectric generators with a low temperature difference between the two sides it is necessary to manage very low voltage and current. Also for standard DC/DC boost converter this is not easy due to the very low amount of voltage and energy available. Thus, we have to increase low voltages (<500 mV) above the minimum threshold required by the boost converter (>2 V). Since our thermoelectric generator produces a voltage between 50 mV and 500 mV, it is necessary to increase more than 40 times this value to permit a good conversion.

In order to simplify the construction of the first prototype, an integrated solution is preferable to reduce cost and to obtain a suitable industrial solution. For these reasons some solutions from Linear Technologies (LT) turned out to be useful because they integrate into a single chip the DC/DC regulator, the charge con-troller, and the main control system, by reducing cost and imple-mentation time. Only few additional components have been selected and added to the integrated chip in order to obtain the fi-nal required solution. An integrated circuit that permits this kind of conversion is the LTC3108 by Linear Technologies; this chip is a boost converter that requires only some external components to work in wide conditions. By using a transformer instead of a gen-eric inductance, it is possible to work with very low input voltages too. In particular, our prototype is equipped with coupled induc-tors with a turns ratio of 1:100 to increase the input voltage; the second stage is given by the boost converter which provides an output voltage which can be set equal to 2.35 V, 3.3 V, 4.1 V, or 5 V to properly supply any kind of microprocessors or sensors. On the other hand, the voltage of the storage system in fixed at the value of 5.25 V. Since the output voltage cannot be greater than the storage voltage, by setting the output voltage at the lowest va-lue it is possible to maximize the available stored energy. The block diagram of the whole energy conversion circuit and the scheme of the equivalent electronic circuits are shown in Figs. 6 and 7, respectively.

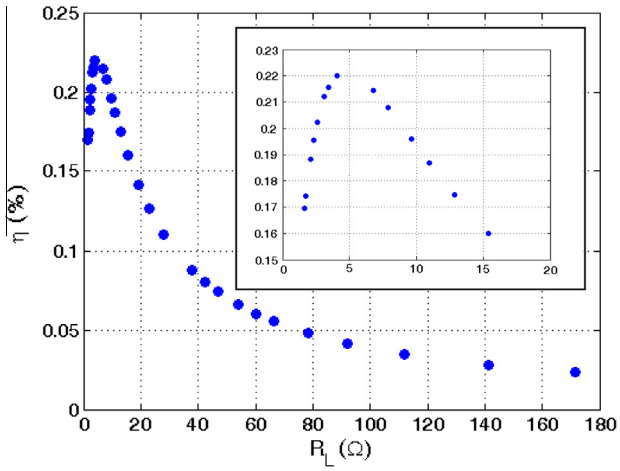


**Fig. 14.** Efficiency $\eta$ as a function of load resistance $R_L$. Inset: magnified view around maximum.

The produced energy can be either directly used by an external load or partially stored for future use. The storage system can be divided in two main components, based on different technologies:

- Electrostatic storage (super capacitors): most suitable when the external load requires small quantity of energy in short intervals (less than 10 min) and the generator continuously supplies the average energy required. The auto-discharge factor is higher than in the chemical solution but in the short period it can be neglected.
- Chemical storage (NiMH batteries): most suitable when the generator has an intermittent production or the external load requires medium/large quantity of energy with long pause interval also when the generator is switched off. The auto-discharge factor is negligible, but the storage efficiency is lower than in the electrostatic storage, by causing efficiency reduction during the charge–discharge cycle.

Both solutions have been tested by using a 4.7 mF 16 V and 330 mF 5.5 V double layer capacitors for the electrostatic storage and a battery pack of 150 mAh 4.8 V for the chemical storage; the chemical solution becomes useful when the energy absorbed by the load is characterized by a long interval of inactivity (>30 min). However, during the experiments we used the electrostatic solution only, by connecting the 4.7 mF 16 V capacitor. The picture of the prototype of the energy conversion circuit is shown in Fig. 8.

## 4. Experimental results

Different measurements have been performed to physically characterize the TEM. To this end, one has to apply the temperature difference ($T_H - T_C$) and subsequently measure the output voltage in different conditions. To correctly realize this goal, one should set $T_H$ and $T_C$ by using a temperature feedback active control in order to keep constant both these two temperatures and the mean temperature inside the TEM during the specified set of measurements, to reduce the effects of temperature on physical quantities [14]. However, since this is not the main aspect of our work, we have characterized the TEM by directly using the prototype of our device, where both $T_H$ and $T_C$ are not adjustable to a fixed known value. On the other hand, we prove that all the physical quantities have been rigorously obtained. In particular, measurements have been performed by considering the circuit shown in Fig. 9, where to the TEG (composed by box, heat source, and TEM previously discussed) we have connected a passive circuit composed by a variable load resistance $R_T$ and a fixed resistance $R_I$, the last one used to measure the current through the correspond-ing voltage drop; therefore, the previously defined resistance $R_L$ corresponds to $R_L = R_T + R_I$.

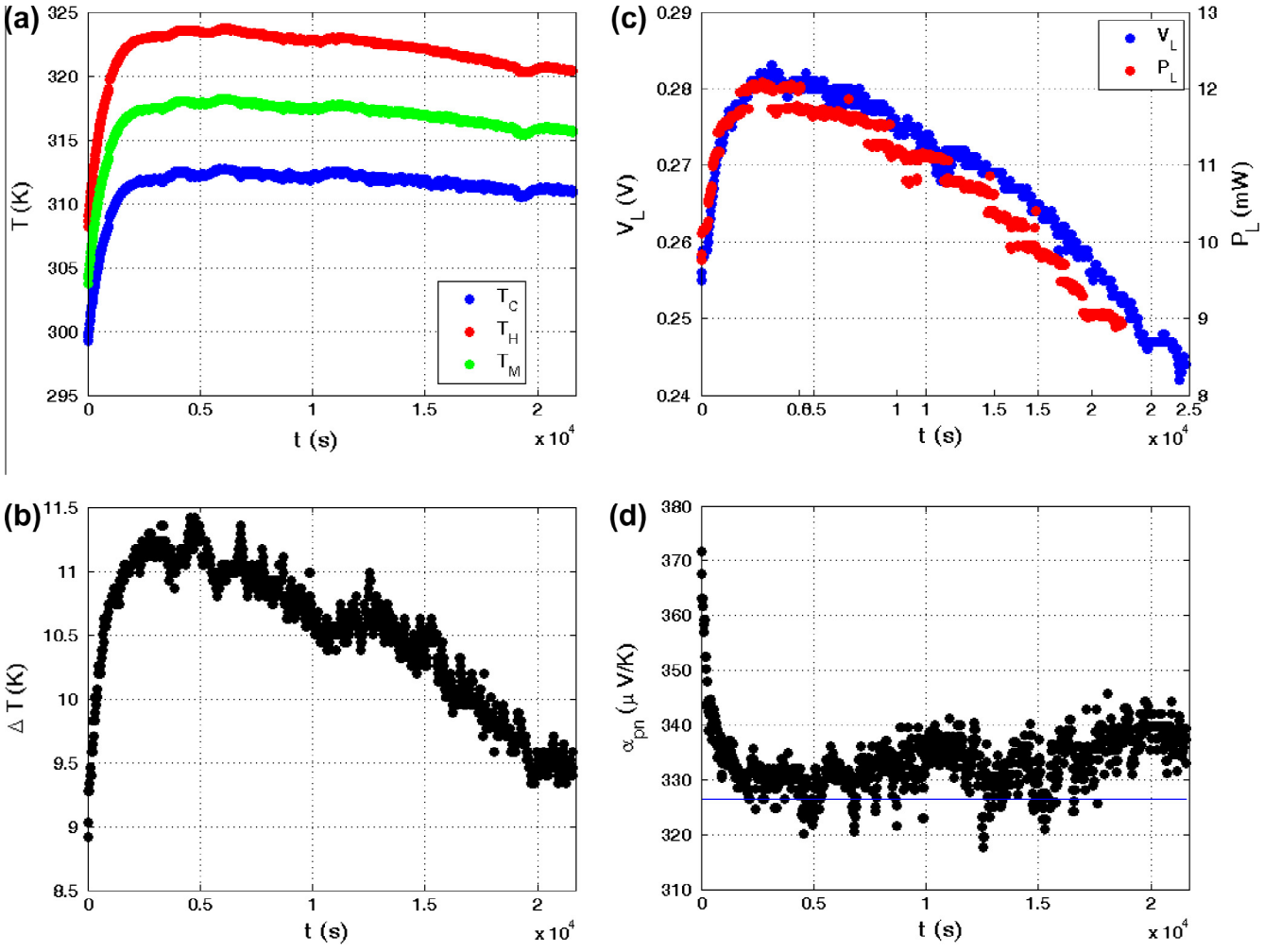


**Fig. 15.** Dependence on time of measured and computed physical quantities obtained during indoor data acquisition at room temperature. (a) $T_C$, $T_H$, and $T_M$; (b) $\Delta T$; (c) $V_L$ and $P_L$; and (d) $\alpha_{pn}$, the horizontal blue line represents the value of Seebeck coefficient computed from power fit. (For interpretation of the references to color in this figure legend, the reader is referred to the web version of this article.)

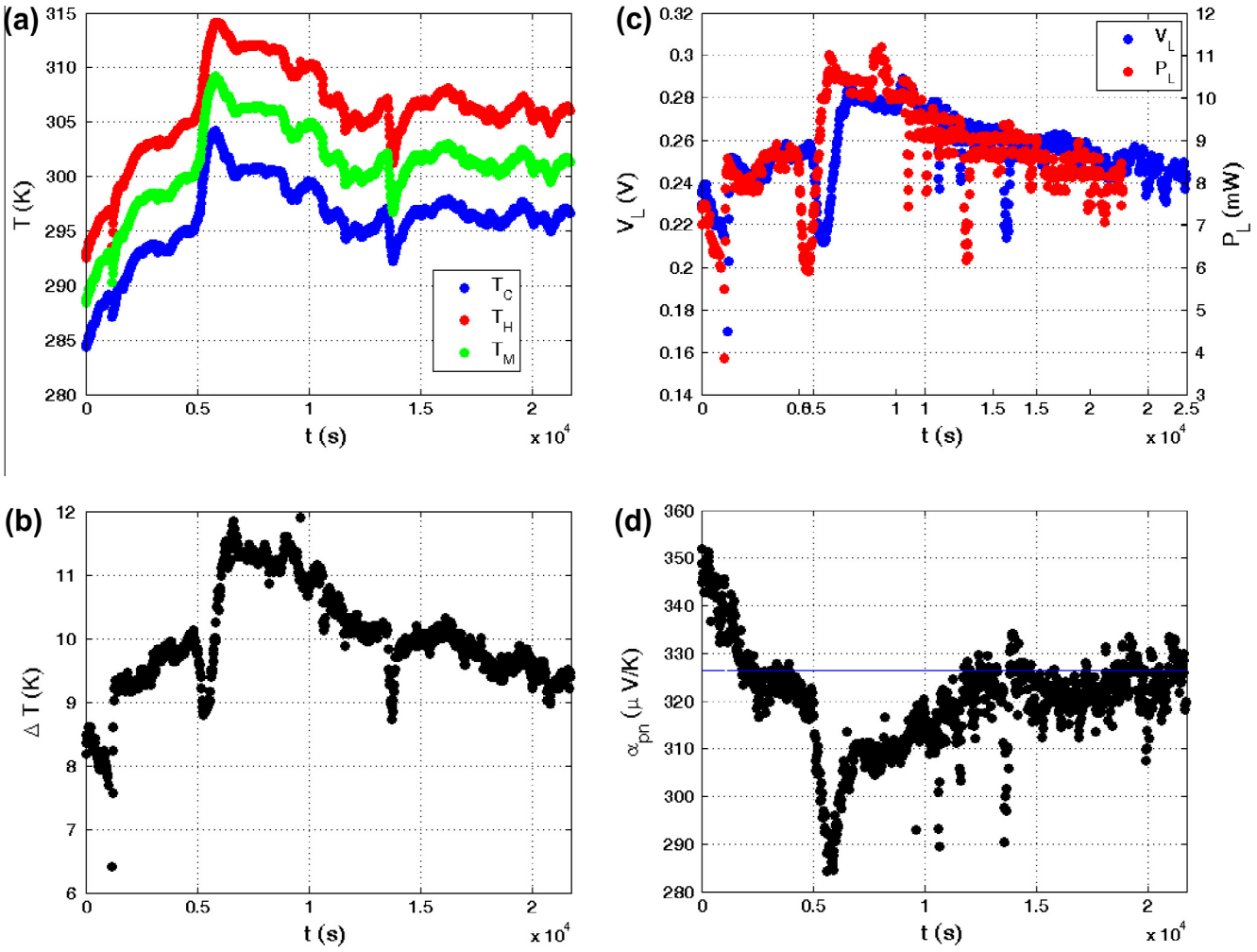


**Fig. 16.** Dependence on time of measured and computed physical quantities obtained during outdoor data acquisition with variable temperature and environmental conditions. (a) $T_C$, $T_H$, and $T_M$; (b) $\Delta T$; (c) $V_L$ and $P_L$; and (d) $\alpha_{pn}$, the horizontal blue line represents the value of Seebeck coefficient computed from power fit. (For interpretation of the references to color in this figure legend, the reader is referred to the web version of this article.)

Computed values from data acquisition are so $\Delta T$, $T_M$, $I$, $R_L = V_L/I$, and $P_L = V_L I$. In Figs. 10 and 11 we show the variation of $T_C$, $T_H$, and $T_M$ and $\Delta T$, respectively, recorded during the experiment, plotted with respect to the variation of the load resistance. In addition, in Fig. 12 we show the variation of $V_L$ and $I$ for the whole $R_L$ values considered during the data acquisition. The dependence of these temperatures with respect to $R_L$ has to be attributed to the fact that the amount of heat exchanged depends on Peltier and Joule effects too, which depend on the load resistance since they are functions of the current.

By plotting $P_L$ versus $R_L$ we are able to determine the required parameters through a data fit, in agreement with Eq. (7). On the other hand, the previously discussed equation of the output power as a function of the load resistance has been obtained by assuming a constant temperature difference $\Delta T$, which is not our case during the whole data acquisition. To overcome this problem, we therefore plot $P_L/\Delta T^2$ versus $R_L$ and then we fit the values with the function $P_L/\Delta T^2 = c_1 R_L/(c_2 + R_L)_2$, being the fitting parameters equal to $c_1 = (N\alpha_{pn}\beta)^2$ and $c_2 = R_{in}$, where we have taken into account the relationship $\Delta T_{eff} = \beta \Delta T$. The result is shown in Fig. 13.

The average of mean temperature inside the TEM and the average of temperature difference around the TEM during this data acquisition are respectively $\langle T_M \rangle = 320.06$ K and $\langle \Delta T \rangle = 11.35$ K (see Figs. 10 and 11, respectively). Data fit provides $c_1 = 1.6631$ mW Ω/K$^2$ and $c_2 = R_{in} = 4.18$ Ω, which is in good

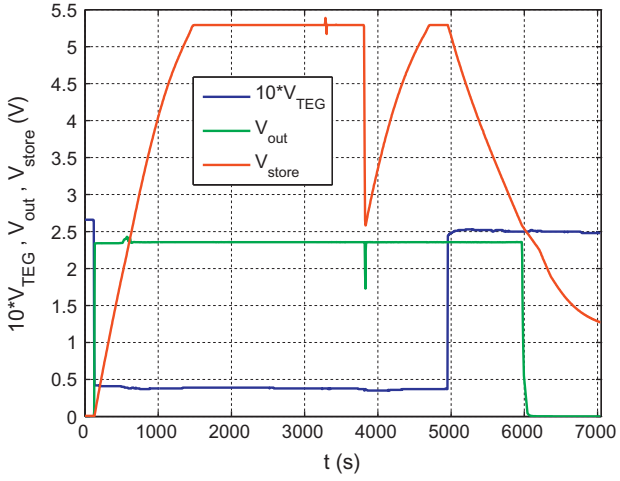


**Fig. 17.** Voltages measured during the test of the whole device as functions of time. Blue line: $V_L$ multiplied by 10; green line: $V_{out}$; red line: $V_{store}$. The voltage drop and rise at 3800 s ca. is when the LED has been connected and disconnected, respectively. The voltage drop at 6000 s ca. is when the external circuit has been disconnected from the TEG. (For interpretation of the references to color in this figure legend, the reader is referred to the web version of this article.)

agreement with that one supplied by the data sheet. In particular, we obtain $\rho_s = 16.82\ \mu\Omega$ m. The accuracy of this fit is guaranteed by the chi-squared test. By considering an error of 0.001 W/K$^2$ for each experimental data plotted in Fig. 13 (error bars are not visible because inside the points), we obtain as reduced chi-squared $\chi^{\hat{}2} = 0.47$, values which confirms, being $\chi^{\hat{}2} < 1$, the accuracy of the fit and the correctness of Eq. (7).

Let us now discuss how we can determine the Seebeck coefficient of a single semiconductor couple. In first approximation, $\beta$ is equal to (see Eq. (8)):

$$\beta \simeq \frac{K}{K + 2K_{in}} = 0.9834, \tag{17}$$

where the contribution from the Peltier effect has been neglected. Therefore, we simply have:

$$\alpha_{pn} = \frac{\sqrt{c_1}}{N\beta} = 326.52\ \mu\text{V/K}, \tag{18}$$

which is in agreement with the values known in literature (see, for comparison, [6,16,15]). Conversely, by rigorously applying the exact expression of $\beta$ given by Eq. (8) we obtain a second order parametric equation for $\alpha_{pn}$ with $R_L$ and $T_M$ as parameters. By solving such equation for each data set we obtain several values of $\alpha_{pn}$, varying from 327.64 μV/K to 326.55 μV/K and with a mean value of 326.96 μV/K. Moreover, the corresponding values of $\beta$ run from 0.9801 to 0.9833. Since the difference with the approximate value is irrelevant, in the sequel we will consider the simplified expres-sion for $\beta$.

Under these considerations, the computation of the figure-of-merit (Eq. (10)) gives rise to $Z = 9.05 \times 10^{-4}$ 1/K, whereas $ZT_M = 0.29$. According to the previous discussion, as stated by Eq.(9), the efficiency varies along the range of load resistance values as shown in Fig. 14. In details, characteristic values are $\eta_{\text{match}} = 0.2205\%$ and $\eta_{\text{MAX}} = 0.2214\%$ (see Eqs. (11) and (12)) against a Carnot efficiency equal to $\eta_C = 3.43\%$, since the averaged temperature values of hot and cold junctions provide $T_{HJ} = T_M + \Delta T/2 = 325.64$ K and $T_{CJ} = T_M - \Delta T/2 = 314.48$ K. It is clear that the efficiency is definitely low, but this fact is due to the relatively low values of temperature difference. With the same figure-of-merit, if we suppose $T_{HJ} = 400$ K and $T_{CJ} = 300$ K we would obtain $\eta_{\text{MAX}} = 1.94\%$.

After this first set of measurements developed to characterize the TEG, we carried out a different type of data acquisitions under similar operative conditions observed during the applications of the thermoelectric element as power generator. In more details, we fixed the resistance load to a well defined value, we turn on the heat source, and then we acquire data every 20 s for 6 h. Such kind of measurements have been implemented both in laboratory, at room temperature, and outdoor, where the temperature and in general the environmental conditions are arbitrary and obviously not adjustable.

The results obtained in the first case are shown in Fig. 15, where all the physical quantities are plotted as functions of time. In this case, we have $R_L = 6.66\ \Omega$. After a fast rise, the temperature $T_H$ at the hot side progressively but slowly decreases, whereas the temperature $T_C$ at the cold side remains basically constant thank to a cooling fan close to the heat sink. Consequently, both the mean temperature $T_M$ and the temperature difference $\Delta T$ have the same functional behavior of $T_H$ (see Fig. 15a and b). It follows that also the output voltage $V_L$ and the output power $P_L$, after a fast rise

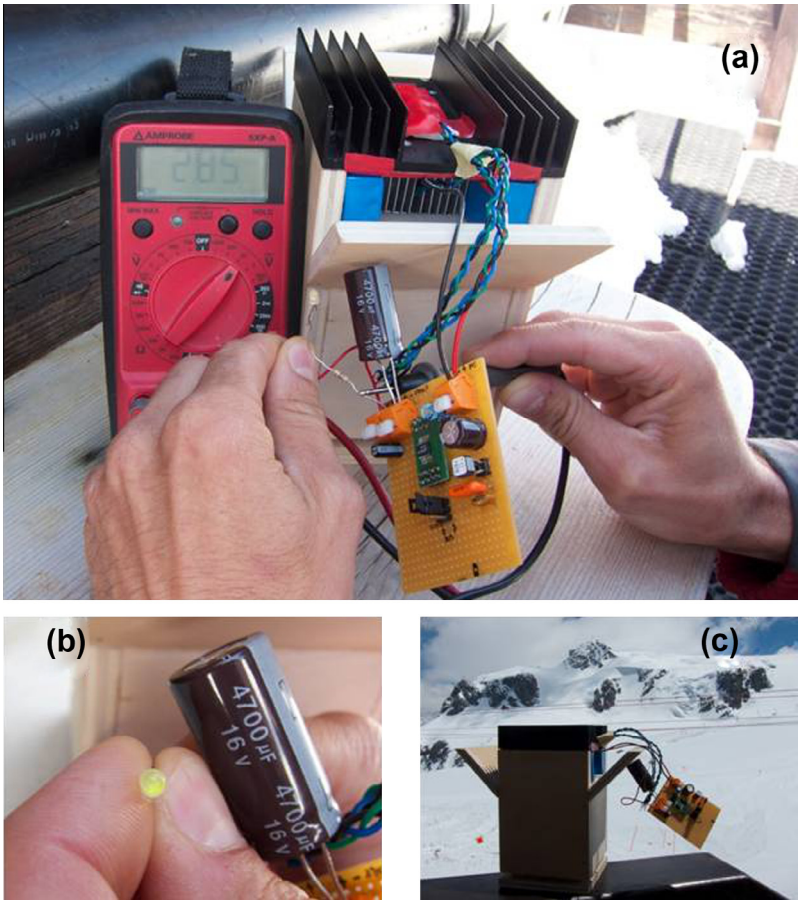


**Fig. 18.** Operative tests in environmental conditions. (a) Value of $V_{out}$ (2.85 V) in open circuit condition; (b) LED lightning; and (c) environmental site of operative tests.

during the transient initial state, decrease as expected from the behavior of $\Delta T$ (see Fig. 15c). Besides, the corresponding efficiency $\eta$ from a value close to 0.22% monotonically drops to 0.18%. It is important to notice that the output voltage is always noticeably higher than 200 mV, a critical value required in several electronic applications, as discussed in the sequel. Finally, from the relationship $V_T = R_{in}I + V_L = N\alpha_{pn}\beta\Delta T$ we were able to compute the Seebeck coefficient at each acquisition time; the result is shown in Fig. 15d where we plotted the value of $\alpha_{pn}$ obtained from the power fit previously discussed. Basically, the variation of $\alpha_{pn}$ is not influent and can be reasonably attributed to a change in the measurement conditions. Such dependence on time of all these quantities can be attributed to the fact that the hot air remains close to the output of the catalytic burner and therefore the reduced absorption of oxygen decreases the heat production.

The same type of measurements has been carried out by placing the TEG outdoor, leaving the device subjected to random environmental conditions (alternation sun-shadow, wind, humidity, etc.). During this data acquisition we set $R_L$ = 7.48 Ω. The results are shown in Fig. 16. With respect to the previous case, here we cannot highlight a common behavior of the variation of the physical quantities since the random change of external conditions is reflected in a random variation of measured and computed parameters. In particular, the external air flow supplies oxygen to the catalytic burner by increasing the efficiency of heat production. It was observed that after a relatively strong air flow $T_H$ immediately decreases be-cause the hot air is removed, but later $T_H$ reaches higher values since the new oxygen increases the heat production. As conse-quence, all the other parameters reflect the same behavior. As one can appreciate by direct comparison of Fig. 15 with Fig. 16, the performances are better when the TEG is placed outdoor, in particular the efficiency is basically higher. Finally, we notice that the first drop at 1020 s was due to the undesired switch off of the heat source.

## 5. Operative tests

Laboratory measurements have been developed to test the whole device, by including the external energy conversion circuit. The results are shown in Fig. 17 where we measured the TEG voltage $V_L$ ($V_{TEG}$ in Fig. 17 since it corresponds to the generated voltage in open circuit conditions), the storage device voltage $V_{store}$ (in this case, the 4.7 mF 16 V capacitor), and the voltage $V_{out}$ generated through the conversion circuit, set at 2.3 V. Once the catalytic burner is switched on, in open circuit conditions $V_L$ goes quickly to its maximum value. Then we connected the external circuit: immediately $V_L$ decreases and $V_{out}$ reaches the set value since it supplies a resistor of 984 kΩ, whereas $V_{store}$ increases up to 5.25 V ca., according to the characteristic time of the capacitor. Later, at 3800 s ca., we connected a LED (forward voltage 2.1 V, current from 3 mA to 10 mA) for few seconds at the external circuit: in that period, as expected, both $V_{out}$ and $V_{store}$ decrease and the LED is switched on until $V_{store} > V_{out}$. When the LED is removed, both $V_{out}$ and $V_{store}$ reach their previous values according to their characteristic times. Finally, when the TEG is disconnected, $V_{store}$ starts to decrease and $V_{out}$ quickly drops when $V_{store} \lesssim V_{out}$, whereas $V_L$ returns at its original value. Such kind of experimental test proves that the TEG is able to cyclically supply low power devices, represented by the LED during these measurements, with a duty cycle determined by the characteristic times of the system.

In order to verify the capability of the device to operate in real environmental conditions, we tested it at the top of Testa Grigia, a summit along the border line between Italy and Switzerland in the Monte Rosa range (coordinates: 45°56′2.03″N–7°42′29.94″E; altitude above the sea level: 3480 m; date: May 25, 2012 – see Fig. 18). Since the use of laboratory instruments was not easily available, we limited the experiment by measuring $V_{out}$ with a portable multimeter and by testing the LED lightning. Fig. 18a and b shows the value of $V_{out}$ (2.85 V) in open circuit condition and the LED which is correctly switched on, respectively. Finally, Fig. 18c shows the environmental site where the device has been tested. To our knowledge, this is the first case in which this type of device is tested in real operative conditions, ready to be used in such hard-environmental situations.

## 6. Conclusion

In this work, we discussed the realization and the characterization of a thermoelectric generator prototype used to power autonomous sensors placed in remote environmental locations. A first set of experimental tests have been carried out in order to obtain the physical parameters which typically characterize the thermoelectric devices (Seebeck coefficient, thermal conductance, internal electrical resistance, emitted power, etc.); the obtained values are in agreement with those ones found in literature for such devices. In particular, we prove that the physical model can be accurately checked by directly making use of our prototype, without using a further experimental setup specifically committed to this aim. Subsequently, we performed a series of measurements directed to test the capability of our device to continuously supply energy to low-power circuits; the results show that the prototype, with a low-cost catalytic heat source, supplies an output voltage larger than 200 mV and an average power close to 9 mW for at least 6 h, when a load resistance close to the internal resistance is connected to the thermoelectric module. Finally, we tested the whole device, given by the TEG connected with an appropriate external energy conversion circuit, showing that it is able to supply low power sensors. In particular, the device has been successfully tested in real hard environmental conditions.

## Acknowledgements

The authors would like to thank P. Pellu for the support in the realization of plywood box and E. Zenerino for the help during the environmental tests.

## References

[1] Rowe D, Min G. J. Power Sources 1998;73:193.
[2] Nuwayhid R, Moukalled F, Noueihed N. Energy Convers Manage 2000;41:891.
[3] Stevens J. Energy Convers Manage 2000;42:709.
[4] Nuwayhid R, Rowe D, Min G. Renew Energy 2003;28:205.
[5] Hatami M, Bauer G, Zhang Q, Kelly P. Phys Rev B 2009;79:174426.
[6] Rowe D. CRC Handbook of Thermoelectrics. CRC Press; 1995.
[7] Anatychuk L, Mikhailovskii V, Konopelnyuk V. IEEE 15th International Conference on Thermoelectrics; 1996. p. 387–9.
[8] Casano G, Piva S. Exp Therm Fluid Sci 2011;35:660.
[9] Chen W-H, Liao C-Y, Hung C-I, Huang W-L. Energy 2012;45:874.
[10] Federici J, Norton D, Bruggemann T, Voit K, Wetzel E, Vlachos D. J Power Sources 2006;161:14691478.
[11] Gou X, Xiao H, Yang S. Appl Energy 2010;87:31313136.
[12] Karri M, Thacher E, Helenbrook B. Energy Convers Manage 2011;52:15961611.[13] Nuwayhid R, Shihadeh A, Ghaddar N. Energy Convers Manage 2005;46:16311643.
[14] Dalola S, Ferrari M, Ferrari V, Guizzetti M, Marioli D, Taroni A. IEEE Trans Instrum Meas 2009;58:99.
[15] Lineykin S, Ben-Yaakov S. IEEE Trans Ind Appl 2007;43:505.
[16] Ahiska R, Ahiska K. Energy Convers Manage 2010;51:338.
[17] Rodriguez A, Vian J, Astrain D, Martinez A. Energy Convers Manage 2009;50:1236.
[18] http://www.zippo.com/product.aspx?id=1023911.
[19] http://www.etdyn.com.